The OSIRIS-REx target asteroid (101955) Bennu: Constraints on its physical, geological, and dynamical nature from astronomical observations

D. S. LAURETTA[1,*], A. E. BARTELS[2], M. A. BARUCCI[3], E. B. BIERHAUS[4], R. P. BINZEL[5],
W. F. BOTTKE[6], H. CAMPINS[7], S. R. CHESLEY[8], B. C. CLARK[9], B. E. CLARK[10],
E. A. CLOUTIS[11], H. C. CONNOLLY[12,13,14], M. K. CROMBIE[15], M. DELBÓ[16], J. P. DWORKIN[2],
J. P. EMERY[17], D. P. GLAVIN[2], V. E. HAMILTON[6], C. W. HERGENROTHER[1], C. L. JOHNSON[18,19],
L. P. KELLER[20], P. MICHEL[16], M. C. NOLAN[21], S. A. SANDFORD[22], D. J. SCHEERES[23],
A. A. SIMON[2], B. M. SUTTER[4], D. VOKROUHLICKÝ[24], and K. J. WALSH[6]

[1]Lunar and Planetary Laboratory, University of Arizona, Tucson, Arizona 85705, USA
[2]NASA Goddard Space Flight Center, Greenbelt, Maryland 20771, USA
[3]Observatoire de Paris, Paris 75014, France
[4]Lockheed Martin Space Systems, Littleton, Colorado 80127, USA
[5]Massachussets Institute of Technology, Cambridge, Massachusetts 02139, USA
[6]Southwest Research Institute, Boulder, Colorado 80302, USA
[7]University of Central Florida, Orlando, Florida 32816, USA
[8]Jet Propulsion Laboratory, Pasadena, California 91109, USA
[9]Space Science Institute, Boulder, Colorado 80301, USA
[10]Ithaca College, Ithaca, New York 14850, USA
[11]University of Winnipeg, Winnipeg MB R3B 2E9, Canada
[12]Kingsborough Community College of CUNY, Brooklyn, New York 11235, USA
[13]The Graduate Center of CUNY, New York, New York 10016, USA
[14]AMNH, Central Park West, New York, New York 10024, USA
[15]Indigo Information Services, Tucson, Arizona 84745, USA
[16]Lagrange Laboratory, University of Nice-Sophia Antipolis, CNRS, Côte d'Azur Observatory, Nice 06300, France
[17]University of Tennessee, Knoxville, Tennessee 37996, USA
[18]Planetary Science Institute, Tucson, Arizona 85719, USA
[19]University of British Columbia, Vancouver, British Columbia V5Z 1M9, Canada
[20]NASA Johnson Space Center, Houston, Texas 77058, USA
[21]Arecibo Observatory, Arecibo 00612, Puerto Rico
[22]NASA Ames Research Center, Mountain View, California 94035, USA
[23]University of Colorado, Boulder, Colorado 80309, USA
[24]Institute of Astronomy, Charles University, 116 36 Praha 1, Czech Republic,
*Corresponding author. E-mail: lauretta@lpl.arizona.edu

Abstract–We review the results of an extensive campaign to determine the physical, geological, and dynamical properties of asteroid (101955) Bennu. This investigation provides information on the orbit, shape, mass, rotation state, radar response, photometric, spectroscopic, thermal, regolith, and environmental properties of Bennu. We combine these data with cosmochemical and dynamical models to develop a hypothetical timeline for Bennu's formation and evolution. We infer that Bennu is an ancient object that has witnessed over 4.5 Gyr of solar system history. Its chemistry and mineralogy were established within the first 10 Myr of the solar system. It likely originated as a discrete asteroid in the inner Main Belt approximately 0.7–2 Gyr ago as a fragment from the catastrophic disruption of a large (approximately 100-km), carbonaceous asteroid. It was delivered to near-Earth space via a combination of Yarkovsky-induced drift and interaction with giant-planet resonances. During its journey, YORP processes and planetary close encounters modified Bennu's spin state, potentially reshaping and resurfacing the asteroid. We also review work on Bennu's future dynamical evolution and constrain its ultimate fate. It is one of the most Potentially Hazardous Asteroids with an approximately 1-in-2700 chance of impacting the Earth in the late 22nd century. It will most likely end its dynamical life by falling into the Sun. The highest probability for a planetary impact is with Venus, followed by the Earth. There is a chance that Bennu will be ejected from the inner solar system after a close encounter with Jupiter. OSIRIS-REx will return samples from the surface of this intriguing asteroid in September 2023.

INTRODUCTION

The **O**rigins, **S**pectral **I**nterpretation, **R**esource **I**dentification, and **S**ecurity **R**egolith **Ex**plorer (OSIRIS-REx) asteroid sample return mission will survey near-Earth asteroid (101955) Bennu to understand its physical, mineralogical, and chemical properties; assess its resource potential; refine the impact hazard; and return a sample of this body to Earth. This mission is scheduled for launch in 2016, rendezvous in 2018, and departure in 2021. Sample return to Earth follows in 2023 (Fig. 1). The primary objectives of the mission are to

1. Return and analyze a sample of pristine carbonaceous asteroid regolith in an amount sufficient to study the nature, history, and distribution of its constituent minerals and organic material;
2. Provide sample context by documenting the regolith at the sampling site in situ at scales down to the subcentimeter;
3. Map the global properties, chemistry, and mineralogy of a primitive carbonaceous asteroid to characterize its geologic and dynamic history and provide context for the returned samples;
4. Understand the interaction between asteroid thermal properties and orbital dynamics by measuring the Yarkovsky effect on a potentially hazardous asteroid and constrain the asteroid properties that contribute to this effect;
5. Improve asteroid astronomy by characterizing the astronomical properties of a primitive carbonaceous asteroid to allow for direct comparison with ground-based telescopic data of the entire asteroid population.

Bennu is an exciting target for an asteroid sample return mission. It is different from all other near-Earth asteroids previously visited by spacecraft. Asteroid (433) Eros, target of the NEAR-Shoemaker mission, and (25143) Itokawa, target of the Hayabusa mission, are both high-albedo, S-type asteroids with irregular shapes. In contrast, Bennu has a very low albedo, is a spectral B-type asteroid, and has a distinct spheroidal shape. While Eros and Itokawa are similar to ordinary chondrite meteorites, Bennu is likely related to carbonaceous chondrites, meteorites that record the history of volatiles and organic compounds in the early solar system.

Here, we describe the results of the astronomical campaign to characterize Bennu. We then develop a hypothesized timeline for Bennu's formation and subsequent evolution over the history of the solar system. In addition to greatly facilitating mission planning, our astronomical campaign allowed us to make significant progress on achieving OSIRIS-REx mission objectives #3, #4, and #5 outlined above.

DISCOVERY AND OBSERVING APPARITIONS

Bennu (provisional designation 1999 RQ36) was discovered on September 11, 1999 by the Lincoln Near-Earth Asteroid Research (LINEAR) survey (Williams 1999). Bennu has a synodic period that results in a close approach to the Earth every 6 yr, providing regular observing opportunities. It was characterized during three apparitions in 1999–2000, 2005–2006, and 2011–2012 when it peaked in brightness at $V = 14.4$, 16.1, and 19.9 magnitudes, respectively. During these apparitions, members of the OSIRIS-REx team and their colleagues conducted an extensive astronomical campaign, measuring a wide range of chemical, physical, and dynamical properties (Table 1).

RESULTS

Orbit Determination and Yarkovsky Effect

Between September 11, 1999 and January 20, 2012, professional and amateur astronomers from around the world made 561 CCD and 29 radar astrometric measurements. Due to this large number of precise plane-of-sky direction (optical astrometry) and line-of-sight distance (radar) measurements, Bennu's orbit is the most precise in the asteroid catalog (Table 2). For example, the formal uncertainty in the semimajor axis is approximately 6 m, the lowest of any known asteroid. Bennu is an Apollo-type NEO with a semimajor axis of 1.126 AU and an eccentricity of 0.204, resulting in perihelion of 0.897 AU and aphelion at 1.36 AU (Fig. 2). The orbital inclination is 6.03° and the orbital period is 1.20 yr. As a result, Bennu makes a close approach to the Earth every 6 yr. This cadence establishes the frequency of observing opportunities as well as the overall OSIRIS-REx mission timeline.

Chesley et al. (2014) determined Bennu's orbit to unprecedented precision using a high-fidelity force model to compute the asteroid's trajectory. One needs to include not only the gravitational effect of the Sun but also that of the eight planets, the Moon, Pluto, and any asteroids that might perturb Bennu's orbit. Chesley et al. (2014) included the four largest asteroids ([1] Ceres, which is officially a dwarf planet, [2] Pallas, [4] Vesta, and [10] Hygeia) plus the next 12 largest Main Belt asteroids. Finally, they added nine more asteroids, which were selected according to an analysis of which ones could most significantly influence the orbit of Bennu. They also modeled the gravitational perturbation caused
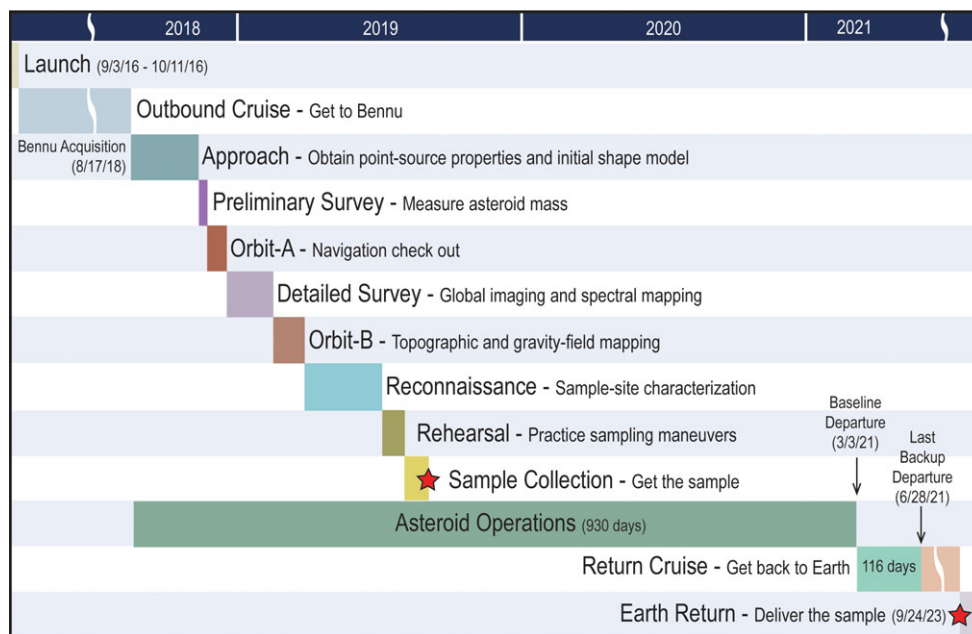
Fig. 1. OSIRIS-REx is a 7-yr journey from launch to Earth Return. The launch window opens in September 2016. After arrival in 2018, nominal sampling is scheduled for late 2019. However, the mission carries substantial operational margin; our departure window opens in March 2021 and extends through late June 2021. Sample return occurs in September 2023.

by the planet's oblateness when Bennu is near the Earth. Unless this effect was included, a modest but discernible error was introduced to the orbit determination and propagation whenever Bennu was closer than 0.3 AU to the Earth. A full relativistic force model was used that included the contribution of the Sun, the planets, and the Moon. The Earth's relativistic terms are responsible for a significant variation in Bennu's trajectory because of short-range perturbations produced during Bennu's close approaches to the Earth in 1999 (0.015 AU) and 2005 (0.033 AU).

The Yarkovsky effect was found to be the most significant nongravitational acceleration acting to alter the asteroid's orbit (Chesley et al. 2014). The Yarkovsky effect is a nongravitational thermal force that results from the way the asteroid rotation affects Bennu's surface-temperature distribution. The absorption of sunlight, and its anisotropic thermal re-emission, can cause a small thrust (Chesley et al. 2003; Bottke et al. 2006). When thermal forces align with orbital velocity vectors, the Yarkovsky effect produces a steady drift in semimajor axis. Measurement of the Yarkovsky acceleration for Bennu is possible because we have obtained three precise series of radar ranging position measurements over a 12 yr period (ten orbits of Bennu around the Sun). The Yarkovsky effect produces a mean rate of change of Bennu's semimajor axis of $-1.90(\pm 0.01) \times 10^{-3}$ AU Myr^{-1}. Since first being observed in 1999, Bennu has drifted over 160 km as a result of this acceleration.

Rotation State, Size, and Shape

We have extensive knowledge on the rotation state, size, and shape of Bennu (Table 3). Lightcurve observations over the nights of September 14–17, 2005 yield a synodic rotation period of 4.2905 ± 0.0065 h (Fig. 3; Hergenrother et al. 2013). The lightcurve amplitude is 0.16 magnitudes. The low amplitude and trimodal (three maxima and three minima) lightcurve is consistent with the rotation of a nearly spherical body observed at high phase angles. Nolan et al. (2013) derived a best-fit shape and pole position for Bennu using a combination of radar images and lightcurve data (Fig. 4). The sidereal rotation period determined from both the lightcurve and radar data is 4.297 ± 0.002 h. Bennu's obliquity is $178 \pm 4°$, with respect to the ecliptic plane, and the rotation pole is at ecliptic coordinates $-88, 45°$ ($\pm 4°$).

The data reveal a spheroidal asteroid undergoing retrograde rotation. The asteroid has a fairly smooth "spinning top" shape with a well-defined equatorial ridge. The long and intermediate axes are 565 ± 10 m and 535 ± 10 m, respectively. The polar diameter is 508 ± 52 m. Due to its shape, Bennu's midlatitude dimensions are significantly smaller than its equatorial and polar dimensions, resulting in a mean diameter of 492 ± 20 m. The shape appears fairly smooth at small scales. There is one 10–20 m boulder on the surface that appears in both 1999 and 2005 radar images, but no other surface features are evident at the radar resolution of 7.5 m.

Table 1. Summary of Bennu observations.

Dates	Telescope + instrument	Observation type
1999		
1999 Sep 15–20	McDonald Obs. 2.1 m	VIS spectroscopy
1999 Sep 23–25	Goldstone 70 m	Radar imaging and ranging
1999 Sep 23, 25, Oct 1	Arecibo 305 m	Radar imaging and ranging
2005–2007		
2005 Sep 4	IRTF + SpeX	NIR spectroscopy
2005 Sep 14–17	Kuiper 1.5 m + CCD	ECAS color and lightcurve photometry
2005 Sep 16, 20, 28, Oct 2	Arecibo 305 m	Radar imaging and ranging
2005 Sep 18–19	Goldstone 70 m	Radar imaging and ranging
2005 Sep–2006 May (8 nights)	Kuiper 1.5 m + CCD	Phase function photometry
2006 Jun 9	VATT 1.8 m + CCD	Phase function photometry
2007 May 3, 4, 8	Spitzer + IRS PUI & IRAC	Thermal spectroscopy and photometry
2011–2012		
2011 Jul 26	Magellan 6.5 m + FIRE	NIR spectroscopy
2011 Aug 13, 29, Sep 14	WHT 4.2 m	Lightcurve photometry
2011 Sep 9	Herschel Space Obs.	Far IR photometry
2011 Sep 27–29	Arecibo 305 m	Radar ranging
2011 Sep–2012 May (13 nights)	Kuiper 1.5 m + Mont4K	Phase function photometry
2012 May 2	Magellan 6.5 m + FIRE	NIR spectroscopy
2012 May 15	VATT 1.8 m + CCD	Phase function photometry
2012 May 19	SOAR 4 m + SOI	Lightcurve and BVR color photometry
2012 Aug 21	Spitzer + IRAC	Thermal photometry
2012 Sep 17–18, Dec 10	HST + WFPC3	Lightcurve photometry

FIRE = Folded-port infrared echellette, HST = Hubble space telescope, IRAC = infrared array camera, IRS PUI = infrared spectrograph "peak-up" imaging channels, IRTF = NASA infrared telescope facility, Mont4K = Montreal 4K CCD imager, SOAR = southern astrophysical research telescope, SOI = SOAR optical imager, SpeX = 0.8–5.5 micron medium-resolution spectrograph, VATT = Vatican advanced technology telescope, WFPC3 = wide-field planetary camera 3, WHT = William Herschel telescope.

Table 2. Bennu's orbital parameters (JPL Solution 85, ecliptic J2000 frame).

Property	Nominal value	1σ uncertainty
Osculating orbital elements		
Reference frame	Sun-centered, Earth ecliptic and equinox of J2000	
Epoch of osculation (ET)	2011 January 1.0 TDB	
Semimajor axis (AU)	1.126391025996	4.2×10^{-11}
Perihelion distance (AU)	0.896894360	2.4×10^{-8}
Aphelion distance (AU)	1.355887692	2.5×10^{-8}
Eccentricity	0.203745112	2.1×10^{-8}
Inclination (°)	6.0349391	2.7×10^{-6}
Long. ascending node (°)	2.0608668	3.7×10^{-6}
Arg. of perihelion (°)	66.230699	5.5×10^{-6}
Epoch of perihelion (ET)	2010-Aug-30.6419464 TDB	0.3 s
Orbital period (days)	436.648727924	2.4×10^{-8}
Yarkovsky effect (10^{-3} AU Myr^{-1})	-1.90	0.01
Impact probability	1 in 2700 between 2175 and 2196	

Albedo, Spectral Properties, and Composition

The geometric visible albedo (pV) of Bennu is well constrained. Using the relationship $2.5 \log pV = 15.62 - 5 \log D - H$, where H is the absolute magnitude (from Hergenrother et al. 2013) and D the asteroid size (from Nolan et al. 2013), constrains pV to $4.5 \pm 0.5\%$. Applying a known correlation between the slope of the linear phase function and the albedo of asteroids (Belskaya and Shevchenko 2000; Oszkiewicz et al. 2011), yields an albedo of 3.0–4.5% based on Bennu's phase function slope of 0.040 mag deg^{-1} (Hergenrother et al. 2013). Near-infrared spectroscopic data show a thermal tail longward of 2 μm (Fig. 5), consistent with an albedo of $4 \pm 1\%$ (Clark et al. 2011). Spitzer photometric measurements combined
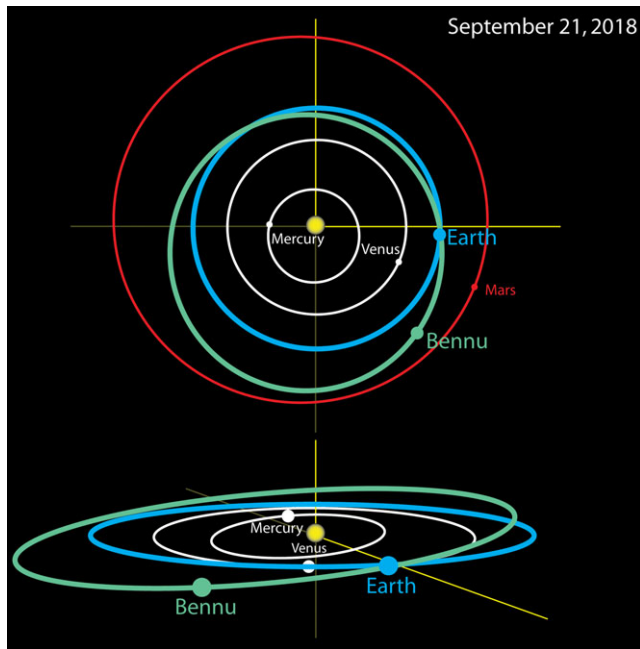
Fig. 2. Orbit diagram for Bennu along with the terrestrial planets looking down from above the North Pole of the Sun (top) and along the ecliptic plane (bottom). The x-axis goes through the vernal equinox. Bennu's orbit was a prime factor in its selection as the OSIRIS-REx target asteroid. Planetary locations are provided during the Approach Phase in September 2018.

Table 3. Bennu size and rotation parameters.

Property	Nominal value	1σ Uncertainty
Size and shape		
Mean diameter (m)	492	20
Polar dimension (m)	508	52
Equatorial dimensions (m)	565 × 535	10
Dynamically equivalent equal volume ellipsoid (DEEVE) dimensions (m)	259 × 251 × 234	10 × 10 × 52
Volume (km^3)	0.0623	0.006
Surface area (km^2)	0.786	0.04
Mass and density		
Bulk density (kg m^{-3})	1260	70
Mass (10^{10} kg)	7.8	0.9
GM (m^3 s^{-2})	5.2	0.6
Hill sphere radius (km)	31.7	+3.3/−4.2
Rotational properties		
Sidereal rotation period (h)	4.297	0.002
Direction of rotation	Retrograde	n/a
Obliquity (°)	178	4
Pole position (°)	(45, −88)	4
Lightcurve amplitude (mag)	0.16	0.05
Nonprincipal axis rotation	No evidence	n/a
Surface and compositional properties		
Geometric albedo (%)	4.5	0.5
Thermal inertia (J m^{-2} s$^{-0.5}$ K^{-1})	310	70
3.5 cm circular polarization ratio, μ$_c$	0.19	0.03
12.6 cm circular polarization ratio, μ$_c$	0.18	0.03
Average slope (°)	15	2.4
Asteroid spectral type	B	n/a
Closest meteorite analogs	CI, CM chondrites	n/a

n/a = not applicable.

with visible photometry constrain the albedo to $4.3 \pm 0.3\%$ (Emery et al. 2014). OSIRIS-REx has adopted a geometric albedo of $4.5 \pm 0.5\%$ for Bennu based on all of these independent determinations.

Visible-to-near-infrared spectroscopy shows that Bennu is a B-type asteroid characterized by a linear, featureless spectrum with bluish to neutral slope (Clark et al. 2011). ECAS color photometry measurements confirm the B-type classification (Hergenrother et al. 2013). Figure 6 presents a comparison of the visible and IR spectra from Clark et al. (2011) with the ECAS photometry from Hergenrother et al. (2013). Both sets of data are consistent within the error bars. The ECAS extension toward the ultraviolet allows some comparison with spectral properties characterized by the Tholen taxonomy (Tholen 1989). Bennu maintains the general spectral qualities of the C-class and its various subtypes (denoted by Tholen as B, C, F), but the UV turnover for Bennu is less pronounced, supporting the B-type designation.

The B-type classification of Bennu permits comparative analysis among other asteroids to infer something about its composition. The B-type asteroids contain many significant objects including (24) Themis (Campins et al. 2010b; Rivkin and Emery 2010) and Main Belt comet 133P/Elst-Pizarro (Hsieh et al. 2004). Bennu is comparable to Themis in spectral properties including albedo, visible spectrum, and near-infrared spectrum from 1.1 to 1.45 μm (Clark et al. 2010). Spectroscopic analysis of Themis shows evidence of H_2O ice and organic material on its surface (Campins et al. 2010b; Rivkin and Emery 2010), suggesting that Bennu has or once had similar compounds. Bennu is also spectrally similar to 133P/Elst-Pizarro and other B-type asteroids in the Main Belt (Hsieh et al. 2004; Hsieh and Jewitt 2006). Some of these objects exhibit periodic cometary activity, suggesting that they contain near-surface volatiles that sublimate when near
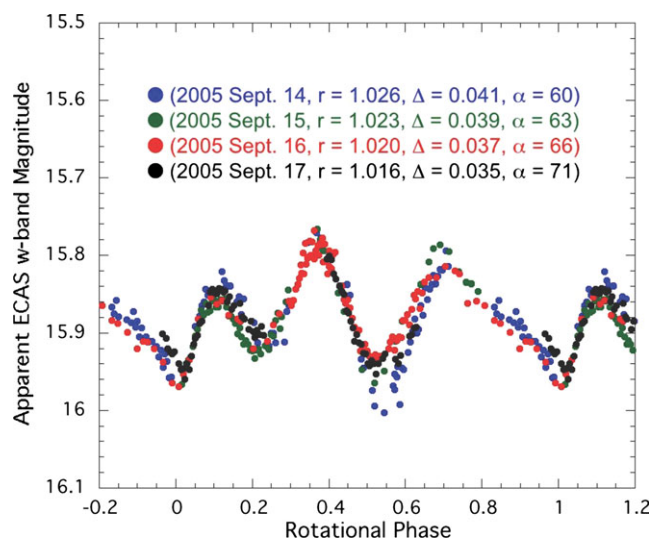
Fig. 3. Composite rotational lightcurve of Bennu from observations made during four consecutive nights in September 2005. These data allow for a high-precision determination of the asteroid's rotation period.

perihelion. Bennu's similarity to these objects supports the hypothesis that it may contain volatile-rich material.

Clark et al. (2011) analyzed the visible and near-infrared spectra of Bennu to constrain composition. They performed a least-squares search for meteorite spectral analogs using 15,000 spectra from the RELAB database. Three best-fit meteorite analogs were identified based on the least-squares search. In addition, six spectral parameters were measured for Bennu and their values compared with the ranges in parameter values of all known carbonaceous chondrite meteorite classes. The results of these least-squares searches and the parametric comparisons suggest that the hydrated CI and CM chondritic meteorites are the most likely analogs for Bennu, reinforcing the interpretation that Bennu is composed of volatile and organic-rich material.

Mass and Density

Radar astronomy probed the upper meter of Bennu, providing constraints on its near-surface density (Nolan et al. 2013). Radar scattering properties are related to composition, density, and material texture of the penetration depth of surface material (Ostro et al. 2004). Using the measured radar albedo of 0.12 and circular polarization ratio of 0.18, coupled with a model for radar interactions with asteroid regolith (Magri et al. 2001), Nolan et al. (2013) found a bulk density of 1650 kg m^{-3} for the material in the upper meter of Bennu. This value compares favorably to the average bulk density of approximately 2100 kg m^{-3} for CI and
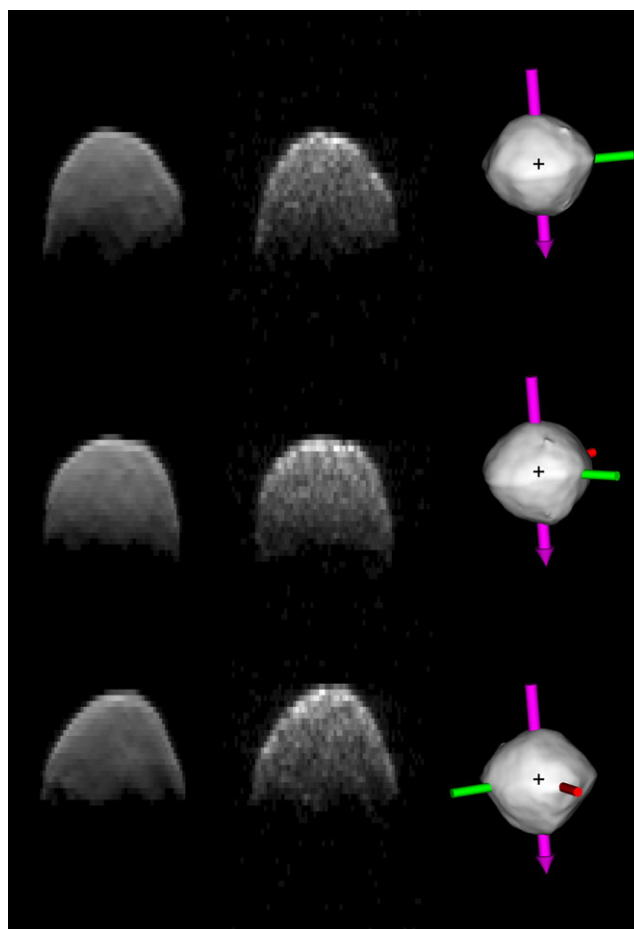

Fig. 4. Radar data collected by the Goldstone and Arecibo planetary radar systems provide detailed images that are used to construct a three-dimensional model of the asteroid and constrain the rotation state. The middle column shows the radar data. The left column shows the model fit to the data. The right column shows the shape model as it would appear on the sky. In the radar frames, the observer is at the top of the frame looking down. The vertical scale is range from the observer in units of 100 ns, or 15 m. The horizontal axis is Doppler shift, or rotation velocity, which, for a solid body, corresponds to linear distance from the rotation axis after projection onto the plane of the sky, and has been scaled to give approximately square pixels.

CM chondritic meteorites, and suggests a low level of porosity near the asteroid surface (approximately 20%).

Radar astrometry combined with infrared astronomy provides an estimate of asteroid mass and, when combined with the shape model, the bulk density of Bennu (Chesley et al. 2014). In particular, the detection of the Yarkovsky effect, combined with observational constraints on the thermal inertia of the body and the radar-derived shape model, allows for an estimate of the mass and bulk density. The drift in semimajor axis due to the Yarkovsky effect is primarily dependent on the body's thermal inertia (Γ), bulk
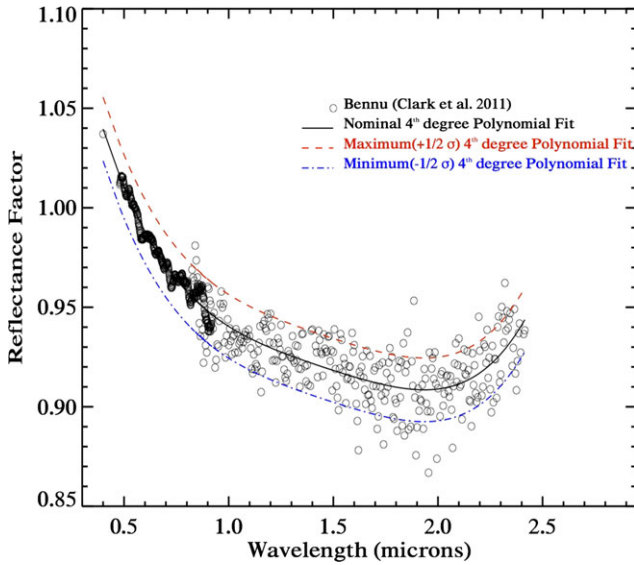
Fig. 5. Visible and near-infrared spectra of Bennu. Smooth spectral curves are fit to the available ground-based spectral data for Bennu from Clark et al. (2011). The increasing reflectance at low wavelengths shows that Bennu is a B-type carbonaceous asteroid. The thermal tail starting at 2-μm wavelength suggests a low albedo.
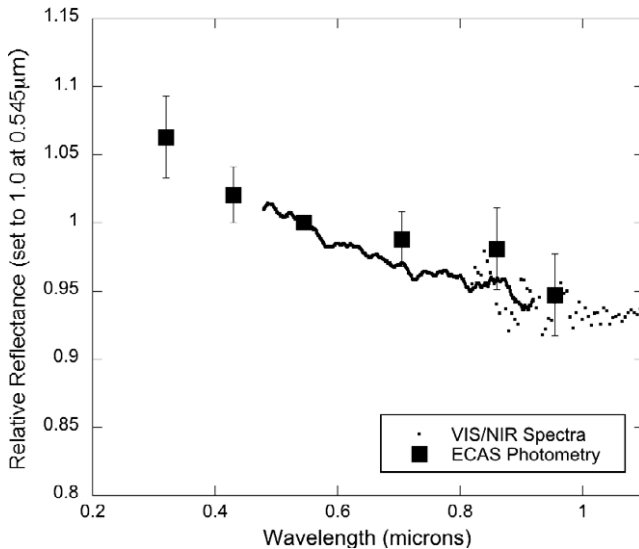

Fig. 6. Comparison of ECAS spectrophotometry from Hergenrother et al. (2013) and visible-to-near-IR spectroscopy from Clark et al. (2011). ECAS filter photometry are consistent with the spectral data and confirms the Btype classification of Bennu.

density (ρ), volume, and obliquity. From radar observations, we have an excellent estimate of the last two of these, while modeling of Spitzer space telescope observations indicates $\Gamma = 310 \pm 70$ J m^{-2} s$^{-0.5}$ K^{-1} (Emery et al. 2014), substantially lower than earlier estimates of this value (Müller et al. 2012). Using these

data and applying a Yarkovsky model leads to a mass estimate of $7.8(\pm 0.9) \times 10^{10}$ kg and a corresponding bulk density of 1260 ± 70 kg m^{-3} (Chesley et al. 2014). This result is the first time that the mass of a planetary object has been measured using a combination of radio astronomy and infrared observations. The low bulk density suggests that Bennu is a rubble-pile asteroid with a macroporosity of approximately 40%.

Regolith Grain Size and Distribution

There are three independent lines of evidence for the particle sizes and regolith distribution on the surface of Bennu: thermal IR measurements using the Spitzer Space Telescope (Emery et al. 2014), radar circular polarization ratio measurements using the planetary radar systems at Goldstone and Arecibo (Nolan et al. 2013), and geophysical analysis of the asteroid shape, density, and rotation state. All data provide high confidence in the presence of regolith on the surface of Bennu.

Spitzer thermal emission data provide firm constraints on the average regolith grain size (Fig. 7a; Emery et al. 2014). Regolith grains that are comparable in size to the thermal skin depth would behave like bedrock. For grain density (2000 kg m^{-3}) and heat capacity (500 J kg^{-1} K^{-1}) values consistent with carbonaceous chondrites and the derived thermal inertia and rotation period of Bennu, the estimated thermal skin depth is approximately 2 cm. For all reasonable assumptions about the density and heat capacity of surface materials, the thermal skin depth on Bennu is <5 cm. The thermal inertia of Bennu is substantially below the bedrock value of >2000 J m^{-2} s$^{-0.5}$ K^{-1}. This difference implies that regolith grains are significantly smaller than the scale of the skin depth and therefore, average less than a centimeter. The rotational coverage of the thermal observations reveals no significant variation in the thermal properties with longitude (Fig. 7b). Bennu's thermal inertia is also substantially lower than that of Itokawa (750–800 J m^{-2} s$^{-0.5}$ K^{-1}), implying that, on average, the grain size on Bennu is smaller than that on Itokawa (Delbo' et al. 2007). This difference is also consistent with the appearance of Itokawa, which looks blocky and cobbled, and the radar shape model of Bennu, which is fairly smooth and devoid of obvious surface features like craters and multiple boulders.

Analysis of the radar circular polarization ratio for Bennu provides an independent constraint on surface grain size. For Bennu, this ratio is 0.18 ± 0.03 for the 12.6 cm wavelength and 0.19 ± 0.03 at the 3.5 cm wavelength (Nolan et al. 2013). These ratios are substantially lower than that for asteroids Itokawa
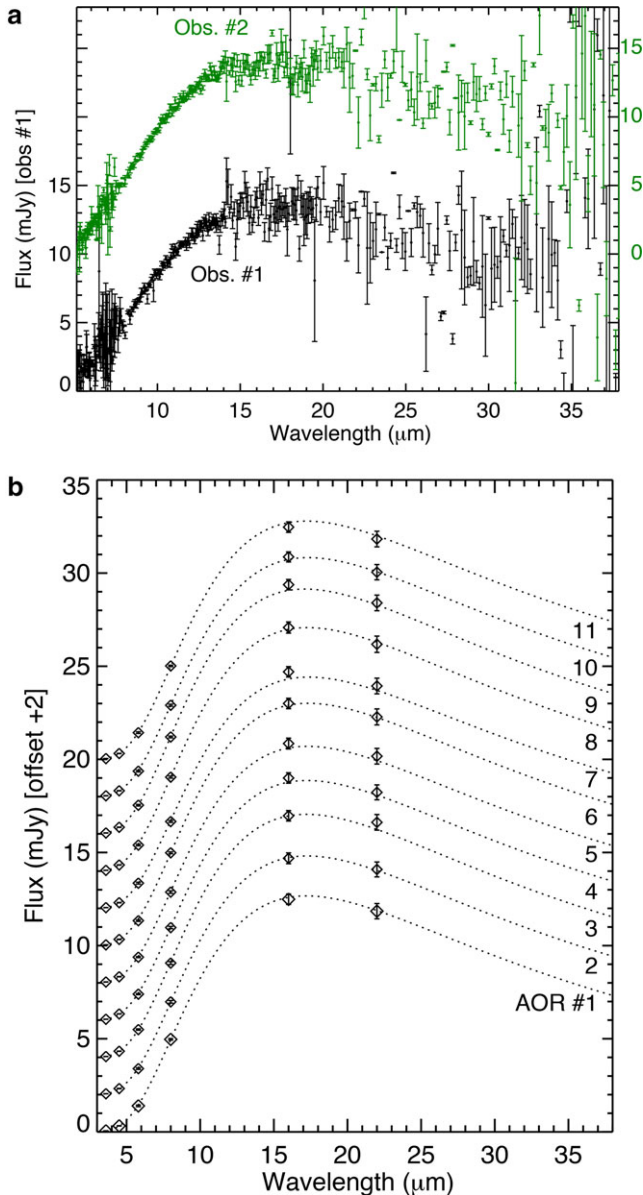
Fig. 7. a) Spitzer/IRS thermal flux spectra of Bennu. The observations were timed to observe opposite hemispheres. The flux scale for the bottom spectrum is on the left axis, and the scale for the top is on the right. b) Spitzer/IRAC and IRS photometric flux observations of Bennu. The observations were timed to obtain data at all six wavelengths at 10 nearly equally spaced longitudes (i.e., every approximately 36° of rotation) with repeat of the first longitude. Fluxes for AOR #1 correspond directly to the left axis and the others all offset by increments of 2 mJy. The dashed lines are model fits to the data.

$(0.26 \pm 0.04$ @ 12.6 cm and 0.47 ± 0.04 @ 3.5 cm) or Eros $(0.28 \pm 0.06$ @ 12.6 cm and 0.33 ± 0.07 @ 3.5 cm), implying that the surface of Bennu is smoother at decimeter spatial scales than either of these two asteroids (Ostro et al. 2004). In addition, the similarity

in circular polarization ratios for Bennu at the two different wavelengths suggests that the transition to a radar "rough" surface happens at a scale smaller than the shortest wavelength (3.5 cm). Itokawa has a higher polarization ratio at 3.5 cm than at 12.6 cm, by a statistically significant factor of almost two. This difference suggests that the particle size distribution on Itokawa is changing at the few-cm scale, and is consistent with the idea that the surface of Itokawa is deficient in particles smaller than about 3.5 cm (Miyamoto et al. 2007), compared to Bennu.

Bennu's shape, dynamic state, and geomorphology provide additional evidence for the presence of loose particulate regolith. Combining the asteroid bulk density with the shape model and rotation state allows us to determine the slope distribution (Fig. 8). The average slope is estimated to be 12.6–17.4°, depending on the bulk density of the asteroid. This subdued slope distribution suggests that there is loose material capable of migrating into geopotential lows. Moreover, the most prominent feature in the shape of Bennu is the equatorial ridge (Fig. 4). This is similar to the structure seen on Asteroid (66391) 1999 KW4 Alpha (Ostro et al. 2006), and is consistent with a migration of material toward the equatorial region (Scheeres et al. 2007). This occurs as the equator becomes the geopotential low for a rapidly rotating body (Guibout and Scheeres 2003). Furthermore, the high slope regions in the midlatitudes of Bennu (Fig. 8) have been shown to be consistent with the migration of material to the equator (Harris et al. 2009). This phenomenon is seen on Itokawa, where the finest grained material has collected in the Muses Sea region of the asteroid (Miyamoto et al. 2007). Over time, if sufficient migration has occurred, gravel may build up a structure at the equator akin to the observed equatorial ridge on Bennu.

Bennu's Environment

The astronomical campaign also provides information on the environment surrounding Bennu, including the presence of natural satellites, as well as dust and gas released from the surface. The lightcurve displays no evidence of satellites (Hergenrother et al. 2013). Radar observations also display no evidence of satellites (Nolan et al. 2013). In addition, the radar data provide firm upper limits on the size of undetected satellites. The radar-detection size limit is dependent on the rotation rate of the satellite and scales with the rotation period to the $-1/3$ power. Using the radar albedo of Bennu and a tidally locked rotation period, the largest undetected satellite within 300 km of Bennu is 2 m. The detection limit for a satellite with the radar albedo of Bennu and a very rapid rotation period
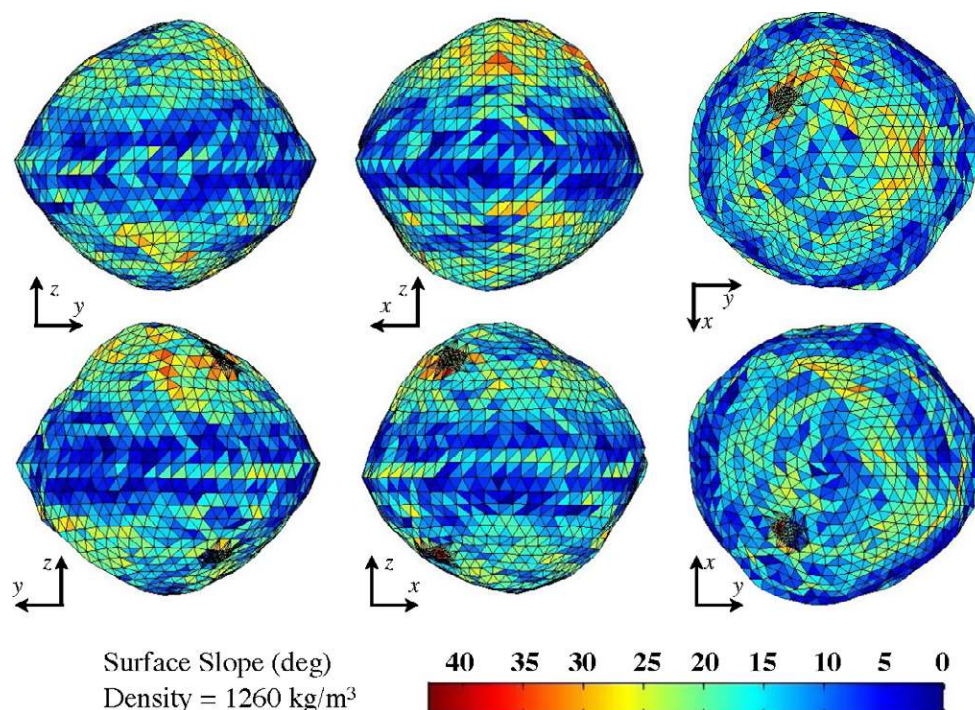
Fig. 8. Bennu shape and slope distribution for the nominal density of 1200 kg m^{-3}. The resolution of the model is increased in both the north and south regions where the detected boulder may be located. The best fit suggests that the boulder is in the southern hemisphere. These models show that the geopotential low of Bennu is along the equator, consistent with the idea that fine-grained regolith has migrated and accumulated in this region of the asteroid.

(0.01 h) is 20 m. Such rapid rotation is common among small near-Earth objects (Pravec and Harris 2000).

We can also constrain the region of space around Bennu where satellite orbits are stable. In order to determine this value, we combine an estimate of the Hill sphere radius ($31.7^{+3.3}_{-4.2}$ km) with solar-radiation pressure effects. The Hill sphere is the radius of the gravitational sphere of influence of Bennu, and is dependent on mass. Solar-radiation pressure is a function of the albedo and the surface area-to-volume ratio of a satellite, producing a size dependence on orbital radii. We find that 1 m satellites are potentially stable out to 26 km, 10 cm satellites out to 16 km, and 1 cm satellites out to 5 km.

Upper limits for dust concentration, dust mass, and dust production rates are based on analysis of Spitzer IR data taken in mid-2007 (Emery et al. 2014). No observations, including Spitzer, have detected dust in the vicinity of Bennu. As a result, we can only set upper limits, defined by the limit of detection of the best Spitzer observations. The upper limit for the concentration of dust within 700 km of Bennu based on the lack of any detectable dust in the Spitzer 16 and 22 μm images is 1.5×10^{19} particles. The upper limit for the mass of dust within 700 km of Bennu is 4×10^{6} g. All of these results suggest minimal hazards, such as satellites or dust, in the OSIRIS-REx operational

environment. OSIRIS-REx will survey this area during the Approach Phase and the derived upper limits on satellites and dust inform the observation planning.

DISCUSSION

The History of Bennu

The great value of asteroid sample return lies in the knowledge of sample context. For OSIRIS-REx, this means both characterization of Bennu at global and local scales during the asteroid encounter as well as determination of Bennu's origin and history. The results of the astronomical campaign have allowed us to develop a detailed hypothetical timeline for the formation and evolution of Bennu and its constituents (Fig. 9).

We infer the earliest history of Bennu's components based on the connection to the CI or CM carbonaceous chondrites (Clark et al. 2011). These samples represent some of the most primitive material from the early solar system. Their oldest minerals formed in the outflows of dying stars such as red giants or supernovae (Fig. 9a; Bernatowicz et al. 2006). These materials were transported through the interstellar medium where they accreted ice mantles and organic compounds (Fig. 9b;
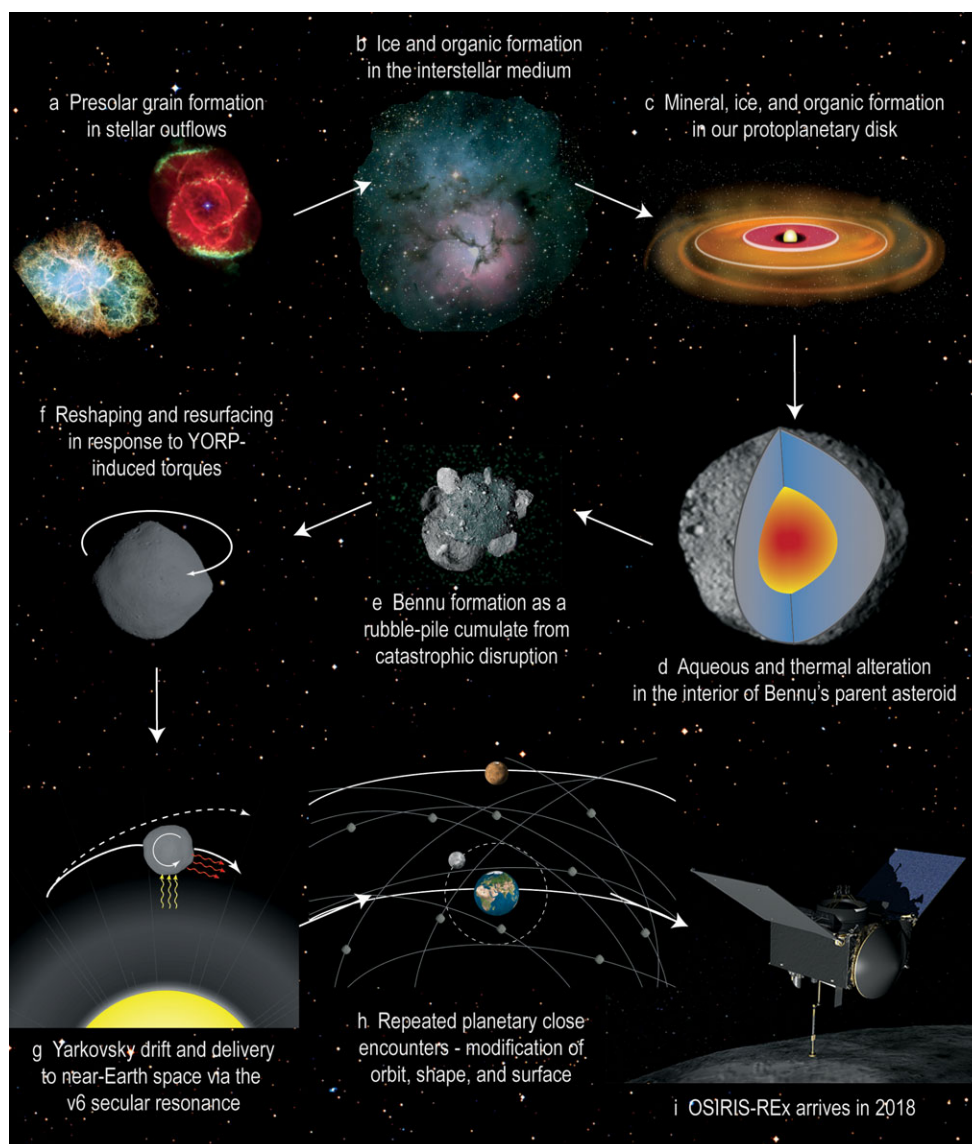
Fig. 9. The hypothesized sequence of events that established the chemistry, mineralogy, shape, and orbit of Bennu. OSIRIS-REx will test and refine this timeline with data from the asteroid encounter and analysis of the returned sample.

Nuth et al. 2006). They were then incorporated into our protoplanetary disk, where they were modified to become the building blocks of the first solar system objects (Fig. 9c; Messenger et al. 2006).

Continuing the inference from carbonaceous chondrites, the next stage of Bennu's history likely involved geologic processing in the interior of a large asteroid (Brearley 2006; Huss et al. 2006). Bennu is probably a fragment of a large Main Belt asteroid (approximately 100 km in diameter) that was shattered in a catastrophic collision. Bodies of this nature formed within the first 10 Myr of the earliest solar system solids. A 100 km asteroid is large enough to retain substantial heat from decay of short-lived radioisotopes,

driving geologic processes such as aqueous alteration and thermal metamorphism (Fig. 9d; Ghosh et al. 2006). These processes may have persisted for tens of millions of years before Bennu's parent asteroid became geologically quiet.

Given that the dynamical lifetime of subkilometer asteroids is short compared to the age of the solar system, Bennu is likely the product of a relatively recent catastrophic asteroid collision (Fig. 9e). Walsh et al. (2013) combined dynamical and spectral information to identify the Main Belt source region of Bennu. By analyzing the low-albedo population of the inner Main Belt, they find that Bennu likely originated from either the Eulalia or the "new" Polana asteroid families,

consistent with the earlier work of Campins et al. (2010a). These analyses indicate that the Eulalia family formed when a 100–150 km asteroid was shattered between 700 and 1500 Myr ago. The new Polana family is more extended in orbital element space and 1000–2000 Myr old. Either of these families could be the source of Bennu. Thus, Bennu likely came into existence as an individual asteroid within the past 0.7–2 Gyr.

Numerical simulations of asteroid catastrophic disruption suggest that most of the resulting fragments are smaller than several hundred meters in diameter (Michel et al. 2001). Bennu's shape and the evidence for loose regolith on its surface suggest that it is a rubble-pile asteroid. These types of objects are thought to form by the reaccumulation of smaller components escaping from the parent asteroid with similar trajectories, leading to a gravitational aggregate (Michel et al. 2001; Bottke et al. 2005).

The current shape and rotation state of Bennu are likely the result of so-called YORP (Yarkovsky–O'Keefe–Radzievskii–Paddack) thermal torques (Fig. 9f). The spinning-top shape of Bennu is shared by many objects in the near-Earth population, such as (66391) 1999 KW4 (Ostro et al. 2006), (311066) 2004 DC (Taylor et al. 2008), (341843) 2008 EV5 (Busch et al. 2011), and (136617) 1994 CC (Brozovic et al. 2011). These shapes are thought to result from a rubble-pile's response to YORP torques. The YORP effect is a "windmill"-like phenomenon related to radiation pressure (from incident, reflected, and re-emitted photons) acting on the asymmetrical shape of an asteroid. YORP can create a torque that modifies the spin vector of small bodies like Bennu. These torques can drive the asteroid obliquity to end states of 0° or 180° and cause the asteroid rotation rate to increase or decrease (Bottke et al. 2006). Modification of rubble-pile asteroids occurs when rotational angular momentum is added or subtracted to the body causing blocks and particles to move in response to the resulting centrifugal forces (Walsh et al. 2008). Thus, YORP may add enough angular momentum to produce downslope movement, mass shedding, and shape changes. In addition to establishing the spinning-top shape, the resulting wide-scale resurfacing may have brought fresh, unweathered material to Bennu's surface.

Recent work provides some evidence of YORP-driven evolution of Bennu. Binzel and DeMeo (2013) detected variations in the spectral slope as a function of latitude on the asteroid surface. These data are consistent with a gradient from pole to equator in composition or grain size. From multiple observations at different aspect angles, they detect a slight but reliable spectral-slope difference between the polar and equatorial regions of Bennu. While observational effects are not yet ruled out as the cause for some differences in slope, if real they could be interpreted as compositional or grain-size effects. Such latitudinal spectral variations are consistent with regolith migration driven by YORP-induced spin up.

Bennu was almost certainly delivered from the inner region of the Main Belt following the well-studied dynamical pathway from the Main Belt to NEO orbits (Bottke et al. 2000, 2002; Campins et al. 2010a; Walsh et al. 2013). Asteroids with retrograde rotations, like Bennu, drift inward as a result of the Yarkovsky effect (Fig. 9g), while prograde rotators will move farther out into the solar system. Bennu appears likely to have come from the ν_6 secular resonance that defines the inner boundary of the Main Belt. This resonance is not only the dominant supplier of NEOs, but it tends to be very good at producing those that have Earth-like orbits, such as Bennu (Bottke et al. 2002).

It is possible to glean insights into the orbital history of Bennu within the terrestrial planet region, based on its current orbit. Delbo' and Michel (2011) demonstrate that the perihelion distance of Bennu has changed with time as a result of close encounters with the terrestrial planets and the influence of orbital resonances with terrestrial and giant planets (Fig. 9h). From these analyses, they conclude that Bennu has a <10% probability of having spent some time in an orbit with perihelion <0.3 AU (smaller than the perihelion of Mercury). The probability increases to more than 50% for perihelion <0.6 AU, and to more than 80% for perihelion <0.8 AU.

The thermal history of the surface of Bennu has likely been strongly affected by this orbital evolution. In its current orbit, temperatures on Bennu's surface peak at approximately 390 K at the equator and approximately 200 K at the poles (Fig. 10). Coupling the orbital evolution with an asteroid thermal model, Delbo' and Michel (2011) found a 50% probability that regions on the surface of Bennu reached temperatures >500 K in the recent past, potentially altering near-surface volatile and organic compounds. The temperature drops rapidly with depth, however, and regolith 3–5 cm deep likely experienced temperatures approximately 100 K below those at the surface, potentially preserving these important materials. In addition, because Bennu is a rubble-pile, close encounters between Bennu and planets like Earth or Venus may have produced sufficient planetary tidal torques to also reshape the asteroid, change its spin rate, and bring fresh, unaltered material to the surface (Richardson et al. 1998).

Based on the hypothesized Bennu timeline outlined above, it is possible that surface material includes both pristine and space-weathered samples. This model

Bennu Thermal Profile: TI = 400, Perihelion (0.89AU)

■ 200-220 ■ 220-240 ■ 240-260 ■ 260-280 ■ 280-300 ■ 300-320 ■ 320-340 ■ 340-360 ■ 360-380 ■ 380-400
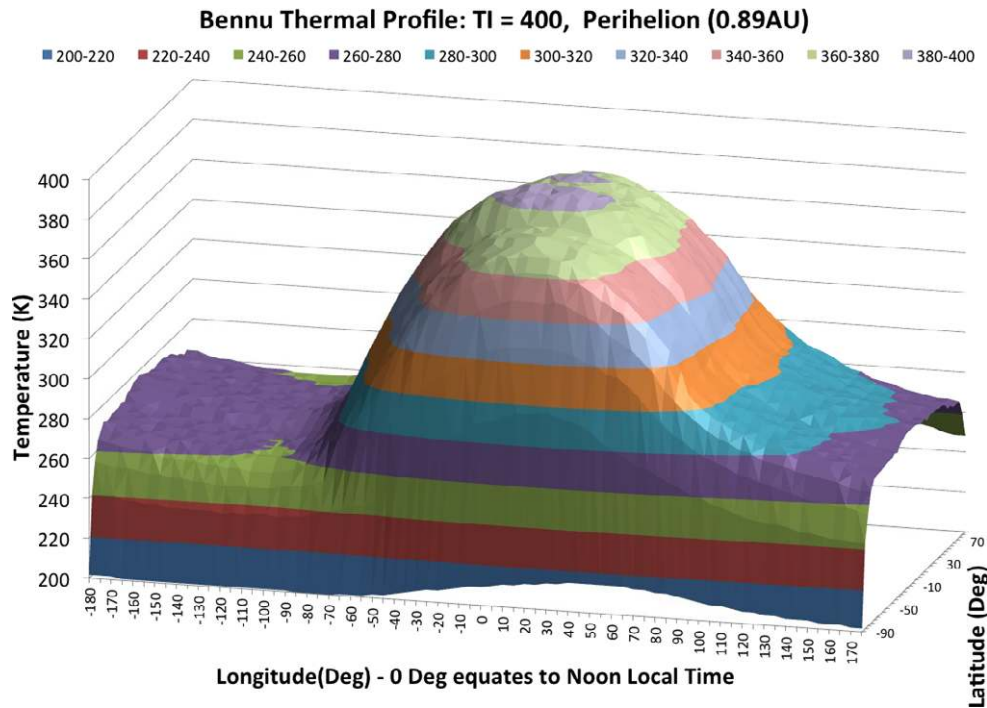
Fig. 10. The worst-case Bennu thermal model. For this case, we use the 1-sigma high-end value for thermal inertia (TI) and place Bennu at perihelion. This model plays a central role in mission planning; the spacecraft must remain within tight thermal tolerances during proximity operations, requiring a detailed thermal model of both the asteroid and the flight system.

provides the basis for the sample analysis strategy for OSIRIS-REx. Analysis of cosmogenic isotope ratios, thermal modification signatures, radionuclide abundances, and nuclear track densities will provide important constraints on the evolution of the parent asteroid and test the hypotheses developed by dynamical studies of Bennu.

Bennu's Future

In addition to reconstructing Bennu's past, we can use our knowledge of the orbit, mass, shape, rotation state, thermal properties, and the Yarkovsky effect to make detailed predictions about Bennu's future. We have a very precise ephemeris for Bennu between 1654 and 2135 (Chesley et al. 2014). In 2135, Bennu will pass 300,000 km (0.002 AU) over the surface of the Earth, inside the orbit of the Moon. This is the last approach that can be predicted without statistical arguments. Beyond 2135, calculations become less deterministic and more statistical in nature, as chaos begins to strongly affect our ability to predict precise perturbations on Bennu's future orbit.

Our knowledge of Bennu's orbit allows us to assess its impact hazard. The Minor Planet Center classifies Bennu as a Potentially Hazardous Asteroid because it has a diameter larger than 150 m and a minimum orbit

intersection distance (MOID) of <0.05 AU with the Earth. Currently, Bennu's MOID is 0.003 AU. The MOID will steadily decrease resulting in a potential Earth impact during the later decades of the 22nd century (Milani et al. 2009; Chesley et al. 2014). Milani et al. (2009) found a cumulative probability of impact of approximately 10^{-3} in the few decades after 2160, with most of the risk associated with a potential Earth encounter in 2182. Incorporating the Yarkovsky effect into the orbital model for Bennu eliminates the 2182 impact hazard. However, the resulting orbital precision increases our knowledge of the likelihood of those potential impacts that persist, as well as revealing new potential impacts in the same timeframe that were previously too remote to resolve. Thus, the tabulation of potential Earth impacts results in a cumulative impact probability of approximately 1 in 2700 sometime in the 2175–2196 time frame (Chesley et al. 2014).

The orbit of Bennu is intrinsically dynamically unstable, as are those of all NEOs. In order to glean probabilistic insights into the future evolution and likely fate of Bennu beyond a few hundred years, we tracked 1000 virtual "Bennus" for an interval of 300 Myr with the gravitational perturbations of the planets Mercury–Neptune included. Our results are consistent with those of Delbo' and Michel (2011) and indicate that Bennu has a 48% chance of falling into the Sun. There is a

10% probability that Bennu will be ejected out of the inner solar system, most likely after a close encounter with Jupiter. The highest impact probability for a planet is with Venus (26%), followed by the Earth (10%) and Mercury (3%). The odds of Bennu striking Mars are only 0.8% and there is a 0.2% chance that Bennu will eventually collide with Jupiter. For certain, Bennu will be visited by OSIRIS-REx starting in 2018.

Impact on Mission Design

The knowledge of Bennu has had a major impact on the design of OSIRIS-REx. The extensive knowledge that exists as a result of our telescopic characterization of Bennu was critical in the selection of this object as the mission target. We have captured this information in a mission-planning document called the Design Reference Asteroid. This document consists of over 100 different asteroid parameters covering orbital, bulk, rotational, radar, photometric, spectroscopic, thermal, regolith, and asteroid environmental properties. This information is used across the project to establish the environmental requirements for the flight system and for overall mission design.

Some of the most important parameters for mission design are the orbit, mass, shape, and rotation state. Combining the derived density with the shape model provides a global asteroid gravity-field model, which allows the team to evaluate the stability of various orbits about the asteroid. The gravity-field model and the rotation state allow us to develop a global surface-slope-distribution model and a global surface-acceleration model (Fig. 8). These models are critical to evaluating our ability to safely deliver the spacecraft to the asteroid surface and maintain a nominal attitude during a 5-s touch-and-go sampling event (Berry et al. 2013). Finally, combining the asteroid shape, rotation state, ephemeris, and albedo yields a global temperature model (Fig. 10), which is critical for ensuring that the spacecraft will not overheat during close approaches to Bennu's surface. All of this information feeds directly into the design of the OSIRIS-REx flight and ground systems, reducing risk and greatly increasing the chances for mission success.

OSIRIS-REx uses a touch-and-go sample acquisition mechanism (TAGSAM) for sample collection. To acquire the bulk sample of regolith, the TAGSAM sampler head releases a jet of N_2 gas that creates a positive pressure area and "fluidizes" the regolith. The N_2 gas and entrained regolith flows through TAGSAM, and the regolith is captured inside the sample collection chamber. This device is capable of ingesting up to 2 kg of material with grain sizes from dust up to 2 cm. This gas-stimulation,

regolith-fluidization technique was chosen for OSIRIS-REx because it is capable of acquiring large amounts of material during a short-duration, 5-s contact with the asteroid surface, minimizes moving parts, functions without motors during sampling, and keeps the sample pristine. This sampling strategy relies on the presence of loose regolith with grain sizes less than 2 cm in longest dimension. The evidence for regolith on the surface as described above provides confidence in our sampling strategy.

Impact on Future Asteroid Science

The measurements made at the asteroid during our encounter will allow us to critically test our pre-encounter understanding of Bennu, built from astronomical observations. A key data product resulting from the asteroid encounter is the Design Reference Asteroid Scorecard. This document will track how well (or poorly) our pre-encounter understanding of Bennu matched reality. In cases where our telescopic observations provided accurate information, we will be able to continue to confidently apply these techniques to other asteroids. However, the most interesting results will be obtained in areas where the ground-based observations proved inaccurate. In these instances, we will be able to use the additional encounter observations to thoroughly review and refine our techniques. The resulting knowledge will improve our ability to characterize small bodies throughout the solar system.

As described above, Bennu's shape and its pole orientation suggest that the YORP effect has affected its morphology. Its orbit and rotation state suggest that Yarkovsky forces have acted to significantly alter its orbit. OSIRIS-REx will provide the first ground-truth assessment of the Yarkovsky and YORP effects as they relate to the chemical nature and dynamical state of an individual asteroid. During encounter, precision tracking of the OSIRIS-REx spacecraft, in combination with modeling of the S/C motion relative to Bennu, will provide the most accurate determination of the Yarkovsky effect ever accomplished, achieving a signal-to-noise ratio >400. This investigation will strongly improve upon the existing measurements derived by Chesley et al. (2014). Detailed measurement of the rotation state during the encounter, compared to the period determined from ground-based lightcurve measurements, will allow us to detect the YORP effect to within 10^{-3} ° day^{-1} yr^{-1}. If this information is combined with previous lightcurve observations, the precision of the detection limit may improve by a factor of approximately five.

OSIRIS-REx will also develop a comprehensive thermophysical model of the asteroid using data

obtained during the asteroid encounter. Comparison of the Yarkovsky and YORP effects predicted from this first-principles approach to the direct measurement of the resulting asteroid acceleration and change in rotation state will test our understanding of these phenomena and lead to a substantial improvement in our knowledge of the fundamental parameters that give rise to these effects. Finally, the thermal conductivity and heat capacity of the returned samples will be directly measured in the laboratory. These fundamental physical parameters, combined with the state of the regolith on the asteroid surface, drive the thermal inertia and the resulting strength of the YORP and Yarkovsky effects. Thus, OSIRIS-REx will benefit future studies of near-Earth objects as well as Main Belt asteroids in many different ways.

SUMMARY

The combination of our astronomical campaign and theoretical modeling has produced a comprehensive model for the formation, evolution, and ultimate fate of Bennu. OSIRIS-REx will return a sample to Earth with unprecedented geologic context and a well-constrained dynamical history. Starting in 2023, worldwide analysis of this material will reveal details and provide constraints on the earliest stages of solar system evolution. In addition, the returned sample will record evidence of the formation of Bennu's parent asteroid, the geologic history of that parent body, the formation of Bennu in a catastrophic collision, and the history of Bennu en route to the inner solar system.

Sample analysis will also enable us to better link Bennu with a specific meteorite group (e.g., CM, CI, or other), understand the chemical inventory of the sample without the uncontrolled exposure to the Earth's biosphere seen by meteorites, and investigate the effects of space weathering on a carbonaceous asteroid. Based on past experience, Bennu is also likely to surprise us. OSIRIS-REx is a mission of exploration. We are heading out to a new world and will return a piece of it to Earth. Just as every previous planetary mission turned up surprises, we should expect similar discoveries from Bennu.

Editorial Handling—Dr. Nancy Chabot

REFERENCES

Belskaya I. N. and Shevchenko V. G. 2000. Opposition effect of asteroids. *Icarus* 147:94–105.

Bernatowicz T. J., Croat T. K., and Daulton T. L. 2006. Origin and evolution of carbonaceous presolar grains in stellar environments. In *Meteorites and the early solar system II*, edited by Lauretta D. S. and McSween H. Y. Tucson, Arizona: University of Arizona Press. pp. 109–126.

Berry K., Sutter B., May A., Williams K., Barbee B. W., Beckman M., and Williams B. 2013. OSIRIS-REx touch-and-go (TAG) mission design and analysis. *36th Annual AAS Guidance and Control Conference*, February 1–February 6, 2013, Breckenridge, Colorado.

Binzel R. P. and DeMeo F. 2013. Latitudinal spectral variations on Asteroid 101955 Bennu. AAS/Division for Planetary Sciences Meeting Abstracts (Vol. 45).

Bottke W. F., Jedicke R., Morbidelli A., Petit J. M., and Gladman B. 2000. Understanding the distribution of near-Earth asteroids. *Science* 288:2190–2194.

Bottke W. F., Morbidelli A., Jedicke R., Petit J. M., Levison H. F., Michel P., and Metcalfe T. S. 2002. Debiased orbital and absolute magnitude distribution of the near-Earth objects. *Icarus* 156:399–433.

Bottke W. F., Durda D. D., Nesvorny D., Jedicke R., Morbidelli A., Vokrouhlicky D., and Levison H. E. 2005. Linking the collisional history of the main asteroid belt to its dynamical excitation and depletion. *Icarus* 179:63–94.

Bottke W. F. Jr., Vokrouhlický D., Rubincam D. P., and Nesvorný D. 2006. The Yarkovsky and YORP effects: Implications for asteroid dynamics. *Annual Review of Earth and Planetary Sciences* 34:157–191.

Brearley A. J. 2006. The action of water. In *Meteorites and the early solar system II*, edited by Lauretta D. S. and McSween H. Y. Tucson, Arizona: University of Arizona Press. pp. 584–624.

Brozovic M., Benner L. A., Taylor P. A., Nolan, M. C., Howell E. S., Magri C., Scheeres D. J., Giorgini J. D., Pollock J. T., Pravec P., Galád A., Fang J., Margot J.-L., Busch M. W., Shepard M. K., Reichart D. E., Ivarsen K. M., Haislip J. B., LaCluyze A. P., Jaoa J., Slade M. A.,

Lawrence K. J., and Hicks M. D. 2011. Radar and optical observations and physical modeling of triple near-Earth Asteroid (136617) 1994 CC. *Icarus* 216:241–256.

Busch M. W., Ostro S. J., Benner L. A., Brozovic M., Giorgini J. D., Jao J. S., Scheeres D. J., Magri C., Nolan M. C., Howell E. S., Taylor P. A., Margot J.-L., and Brisken W. 2011. Radar observations and the shape of near-Earth Asteroid 2008 EV5. *Icarus* 212:649–660.

Campins H., Morbidelli A., Tsiganis K., de León J., Licandro J., and Lauretta D. 2010a. The origin of Asteroid 101955 (1999 RQ36). *The Astrophysical Journal Letters* 721:L53–L57.

Campins H., Hargrove K., Pinilla-Alonso N., Howell E. S., Kelley M. S., Licandro J., Mothé-Diniz T., Fernández Y., and Ziffer J. 2010b. Water ice and organics on the surface of the asteroid 24 Themis. *Nature* 464:1320–1321.

Chesley S. R., Ostro S. J., Vokrouhlický D., Čapek D., Giorgini J. D., Nolan M. C., Margot J. L., Hine A. A., Benner L. A. M., and Chamberlin A. B. 2003. Direct detection of the Yarkovsky effect by radar ranging to asteroid 6489 Golevka. *Science* 302:1739–1742.

Chesley S. R., Farnocchia D., Nolan M., Vokrouhlický D., Chodas P. W., Milani A., Spoto F., Benner L. A., Bottke W. F., Busch M. W., Emery J. P., Howell E. S., Lauretta D. S., Margot J., Rozitis B., and Taylor P. A. 2014. Orbit and bulk density of the OSIRIS-REx target asteroid (101955) Bennu. *Icarus* 235:5–22.

Clark B. E., Ziffer J., Nesvorný D., Campins H., Rivkin A. S., Hiroi T., Barucci M. A., Fulchignoni M., Binzel R. P., Fornasier S., DeMeo F., Ockert-Bell M. E., Licandro J., and Mothé-Diniz T. 2010. Spectroscopy of B-type asteroids: Subgroups and meteorite analogs. *Journal of Geophysical Research-Planets* 115:E6.

Clark B. E., Binzel R. P., Howell E. S., Cloutis E. A., Ockert-Bell M., Christensen P., Barucci M. A., DeMeo F., Lauretta D. S., Connolly H. Jr., Soderberg A., Hergenrother C., Lim L., Emery J., and Mueller M. 2011. Asteroid (101955) 1999 RQ36: Spectroscopy from 0.4 to 2.4 mu m and meteorite analogs. *Icarus* 216:462–475.

Delbo' M. and Michel P. 2011. Temperature history and dynamical evolution of (101955) 1999 RQ36: A potential target for sample return from a primitive asteroid. *The Astrophysical Journal Letters* 728:L42.

Delbo' M., Harris A. W., Mottola S., and Mueller M. 2007. Thermal inertia of near-Earth asteroids and implications for the magnitude of the Yarkovsky effect. *Icarus* 190:236–249.

Emery J. P., Fernández Y. R., Kelley M. S., Crane K. T., Hergenrother C. W., Lauretta D. S., Drake M. J., Campins H., and Ziffer J. 2014. Thermal infrared observations and thermophysical characterization of OSIRIS-REx target asteroid (101955) Bennu. *Icarus* 234:17–35.

Ghosh A., Weidenschilling S. J., McSween H. Y. Jr., and Rubin A. 2006. Asteroidal heating, and thermal stratification of the asteroid belt. In *Meteorites and the early system solar II*, edited by Lauretta D. S. and McSween H. Y. Tucson, Arizona: University of Arizona Press. pp. 555–566.

Guibout V. and Scheeres D. J. 2003. Stability of surface motion on a rotating ellipsoid. *Celestial Mechanics & Dynamical Astronomy* 87:263–290.

Harris A. W., Fahnestock E. G., and Pravec P. 2009. On the shapes and spins of "rubble pile" asteroids. *Icarus* 199:310–318.

Hergenrother C. W., Nolan M. C., Binzel R. P., Cloutis E. A., Barucci M. A., Michel P., Scheeres D. J., d'Aubigny C. D., Lazzaro D., Pinilla-Alonso N., Campins H., Licandro J., Clark B. E., Rizk B., Beshore E. C., and Lauretta D. S. 2013. Lightcurve, color and phase function photometry of the OSIRIS-REx target asteroid (101955) Bennu. *Icarus* 226:663–670.

Hsieh H. H. and Jewitt D. 2006. A population of comets in the main asteroid belt. *Science* 312:561–563.

Hsieh H. H., Jewitt D. C., and Fernández Y. R. 2004. The strange case of 133P/Elst-Pizarro: A comet among the asteroids. *The Astronomical Journal* 127:2997.

Huss G. R., Rubin A. E., and Grossman J. N. 2006. Thermal metamorphism in chondrites. In *Meteorites and the early solar system II*, edited by Lauretta D. S. and McSween H. Y. Tucson, Arizona: University of Arizona Press. pp. 567–586.

Magri C., Consolmagno G. J., Ostro S. J., Benner L. A. M., and Beeney B. R. 2001. Radar constraints on asteroid regolith properties using 433 Eros as ground truth. *Meteoritics & Planetary Science* 36:1697–1709.

Messenger S., Sandford S., and Brownlee D. 2006. The population of starting materials available for solar system construction. In *Meteorites and the early solar system II*, edited by Lauretta D. S. and McSween H. Y., Tucson, Arizona: University of Arizona Press. pp. 187–208.

Michel P., Benz W., Tanga P., and Richardson D. C. 2001. Collisions and gravitational reaccumulation: Forming asteroid families and satellites. *Science* 294:1696–1700.

Milani A., Chesley S. R., Sansaturio M. E., Bernardi F., Valsecchi G. B., and Arratia O. 2009. Long term impact risk for (101955) 1999 RQ(36). *Icarus* 203:460–471.

Miyamoto H., Yano H., Scheeres D. J., Abe S., Barnouin-Jha O., Cheng A. F., Demura H., Gaskell R. W., Hirata N., Ishiguro M., Michikami T., Nakamura A. M., Nakamura R., Saito J., and Sasaki S. 2007. Regolith migration and sorting on asteroid Itokawa. *Science* 316:1011–1014.

Müller T. G., O'Rourke L., Barucci A. M., Pal A., Kiss C., Zeidler P., Altieri B., Gonzalez-Garcia B. M., and Kuppers M. 2012. Physical properties of OSIRIS-REx target asteroid (101955) 1999 RQ(36). *Astronomy & Astrophysics* 548:A36.

Nolan M. C., Magri C., Howell E. S., Benner L. A. M., Giorgini J. D., Hergenrother C. W., Hudson R. S., Lauretta D. S., Margot J.-L., Ostro S. J., and Scheeres D. J. 2013. Shape model and surface properties of the OSIRIS-REx target asteroid (101955) Bennu from radar and lightcurve observations. *Icarus* 226:629–640.

Nuth J. A. III, Charnley S. B., and Johnson N. M., 2006. Chemical processes in the interstellar medium: Source of the gas and dust in the primitive solar nebula. *Meteorites and the early solar system II*, edited by Lauretta D. S. and McSween H. Y. Tucson, Arizona: University of Arizona Press. pp. 147–167.

Ostro S. J., Benner L. A. M., Nolan M. C., Magri C., Giorgini J. D., Scheeres D. J., Broschart S. B., Kaasalainen M., Vokrouhlicky D., Chesley S. R., Margot J. L., Jurgens R. F., Rose R., Yeomans D. K., Suzuki S., and De Jong E. M. 2004. Radar observations of asteroid 25143 Itokawa (1998 SF36). *Meteoritics & Planetary Science* 39:407–424.

Ostro S. J., Margot J.-L., Benner L. A. M., Giorgini J. D., Scheeres D. J., Fahnestock E. G., Broschart S. B., Bellerose J., Nolan M. C., Magri C., Pravec P., Scheirich

P., Rose R., Jurgens R. F., De Jong E. M., and Suzuki S. 2006. Radar Imaging of binary near-Earth asteroid (66391) 1999 KW4. *Science* 314:1276–1280.

Oszkiewicz D. A., Muinonen K., Bowell E., Trilling D., Penttila A., Pieniluoma T., Wasserman L. H., and Enga M. T. 2011. Online multi-parameter phase-curve fitting and application to a large corpus of asteroid photometric data. *Journal of Quantitative Spectroscopy & Radiative Transfer* 112:1919–1929.

Pravec P. and Harris A. W. 2000. Fast and slow rotation of asteroids. *Icarus* 148:12–20.

Richardson D. C., Bottke W. F., and Love S. G. 1998. Tidal distortion and disruption of Earth-crossing asteroids. *Icarus* 134:47–76.

Rivkin A. S. and Emery J. P. 2010. Detection of ice and organics on an asteroidal surface. *Nature* 464:1322–1323.

Scheeres D. J., Abe M., Yoshikawa M., Nakamura R., Gaskell R. W., and Abell P. A. 2007. The effect of YORP on Itokawa. *Icarus* 188:425–429.

Taylor P. A., Margot J. L., Nolan M. C., Benner L. A. M., Ostro S. J., Giorgini J. D., and Magri C. 2008. The shape, mutual orbit, and tidal evolution of binary near-Earth Asteroid 2004 DC. LPI Contribution 1405. Houston, Texas: Lunar and Planetary Institute. 8322 p.

Tholen D. J., 1989. Asteroid taxonomic classifications. *Asteroids II*, edited by Binzel R. P., Gehrels T., and Matthews M. S. Tucson, Arizona: University of Arizona Press. pp. 1139–1150.

Walsh K. J., Richardson D. C., and Michel P. 2008. Rotational breakup as the origin of small binary asteroids. *Nature* 454:188–191.

Walsh K. J., Delbo' M., Bottke W. F., Vokrouhlický D., and Lauretta D. S. 2013. Introducing the Eulalia and new Polana asteroid families: Re-assessing primitive asteroid families in the inner Main Belt. *Icarus* 225:283–297.

Williams G.V., 1999. 1999 RQ36. *Minor Planet Electronic Circular* 1999-R44. http://www.minorplanetcenter.net/iau/mpec/J99/J99R44.html.